ELSEVIER

Journal of Structural Geology 28 (2006) 431–443

JOURNAL OF STRUCTURAL GEOLOGY

www.elsevier.com/locate/jsg

An example of inversion in a brittle shear zone

S. Bigi *

Dipartimento Scienze della Terra, Università degli Studi di Roma, "La Sapienza" Piazzale Aldo Moro 5, 00185 Rome, Italy

Received 5 October 2004; received in revised form 9 December 2005; accepted 22 December 2005

Abstract

A useful tool to document structural inversion inside a shear zone is the identification of overprinted structures, which can increase the complexity of the internal fabric of shear zones. In the case of thrust faults, shear zones can also be problematic due to the occurrence of structures connected to flexural slip along bedding in the recumbent forelimb. Therefore identification of superimposition among different structures can help to distinguish among these configurations inside a shear zone. In Central Apennines (Italy), favourable conditions along the outcrop of Mt. Tancia's thrust allowed the discovery of two sets of superimposed fabric elements referring to two opposite senses of shear. The first is related to thrusting (top-to-E–NE), whereas the second is likely associated to reactivation in normal sense (top-to-W–SW). The fabric elements have been mapped and their distribution inside a semi-brittle shear zone has been defined. High angle extensional shear planes occurring only in the uppermost part of the shear zone (closest to the main thrust plane) have been interpreted as a new generation of C-planes, connected to negative reactivation, instead of Riedel shear planes. The overprinting relationship defined inside the shear zone helps in discriminating whether the observed structures developed in the footwall of the main thrust or on the recumbent limb of the hanging wall's anticline. The deformation inside the shear zone can be described using a simple shear model at the outcrop scale, where reoccurrence of fibrous calcite on shear C-planes should control rotation of S-planes; these are dissolution planes parallel to the XY-plane of the local strain ellipsoid. At thin section scale, instead, veins maintaining the same orientation suggest a coaxial deformation due to repeated crystallization events controlled by fluid pressure and differential stress variation.

Keywords: Brittle shear zones; Tectonites; Apennines; Negative inversion

1. Introduction

Structural reactivation is a fundamental feature of deformation in continental lithosphere. Faulting produces zones of weakness that tend to repeatedly accommodate successive crustal strain. Thrust fault reactivation by a subsequent normal fault is defined as negative inversion (after Williams et al., 1989), and has been largely documented by seismic analysis, field studies and analogue modelling in orogenic belts where an extensional regime follows the contractional one (Malavielle, 1987; Powell and Williams, 1989; Ivins et al., 1990; Faccenna et al., 1995, and many others). Reactivation and/or structural inversion can be also documented using geometries and relative chronology of structures inside the shear zones, as pointed out by several authors (Sibson, 1977; Holdsworth, 1994; Beeson et al., 1995; Butler et al., 1995; Wennberg, 1996; Worley and Wilson, 1996; Holdsworth et al., 1997; Nyman, 1999; Maruyama and Lin, 2004). A useful tool is the recognition of overprinted structures, or changes in the distribution and nature of deformation products within faults and/or shear zone. Changes in shear direction can increase the complexity of internal fabric resulting in a huge number of different configurations and combinations of structures. Moreover, in the case of thrust faults connected to fold development, shear zones can also be complicated by the occurrence of structures connected to flexural slip along bedding in the recumbent forelimb. Identification of superimposition among different structures inside a shear zone can help in distinguishing among these configurations and classifying combinations of sets of compatible structures in order to better define deformation mechanisms, strain regime and deformation chronology.

In the Central Apennines, favourable conditions along the outcrop of Mt. Tancia's thrust allowed the recognition, classification and localization inside a semi-brittle shear zone of several sets of fabric elements both at outcrop and at thin-section scale. Superimposition of two sets of fabric elements referring to two opposite senses of shear have been recognized

* Tel.: +39 06 49914922; fax: +39 06 4454729.
E-mail address: sabina.bigi@uniroma1.it

0191-8141/$ - see front matter © 2006 Elsevier Ltd. All rights reserved.
doi:10.1016/j.jsg.2005.12.012

inside Mt. Tancia's shear zone. High angle extensional shear planes occurring in the uppermost part of the shear zone (closest to the main thrust plane) have been interpreted as a new generation of C-planes, connected to negative reactivation, rather than Riedel shear planes. This interpretation is based on these planes' relationship with the other structures inside the shear zone and on their spatial distribution. Moreover, these data suggest that the resulting fabrics can be explained by a complex interaction between the imposed kinematics and the geometry of the main thrust plane. The overprint relationship defined inside the shear zone allows us to distinguish whether the observed structures developed in the footwall of the main thrust or on the recumbent limb of the hanging wall's anticline.

2. Geological background

The N–S-trending Mt. Tancia's thrust front is located in the western sector of the Central Apennines fold and thrust belt, deformed from Oligocene to Recent (Fig. 1). The stratigraphy is represented by a pelagic succession from Upper Liassic to Miocene, and is characterized by well stratified limestone and cherts, with inter-bedded carbonate turbidites (Civitelli et al., 1986). Mt. Tancia's thrust is part of the Mt. Sabini structure,

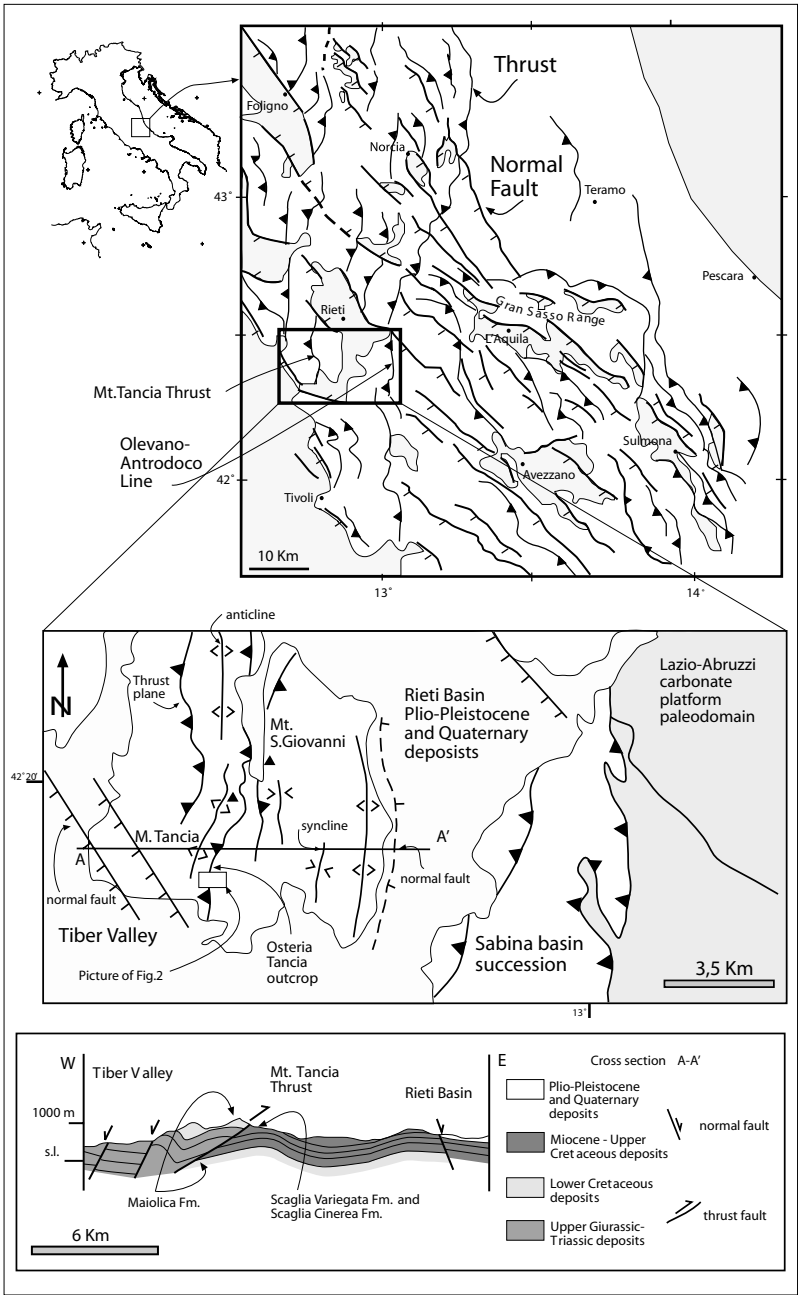

Fig. 1. (a) Structural map of Central Italy. The study area is located in the box. (b) Geological cross-section of Mt. Tancia structure. The cross-section shows the geometry of Mt. Tancia's thrust in the north of studied outcrop. It is possible to estimate an offset of about 3000 m along the thrust fault.

consisting of an asymmetric anticline, with the recumbent eastern limb. A fault-propagation fold model has been proposed to describe the geometry and kinematic evolution of the Mt. Sabini's structure (Cosentino and Parotto, 1992). The timing of the deformation proposed for this area highlights a main compressive phase during the Late Tortonian–Early Messinian time and an 'out of sequence' reactivation during the Early Pliocene (Cavinato et al., 1986). The Mt. Sabini's thrust is offset by the normal fault system of the Tiber Valley in the west, and of the Rieti basin in the northeast. These normal faults strike generally NW–SE and they define a basin filled by the Upper Pliocene–Pleistocene marine and continental deposits belonging to the post-orogenic cycle (Cavinato et al., 1989).

Mt. Tancia's thrust zone crops out South of Rieti (Figs. 1 and 2). The hanging wall consists of Jurassic–Lower Cretaceous rocks (Corniola Fm.–Maiolica Fm.), whereas the marls of Scaglia Variegata and Scaglia Cinerea Formations (Eocene–Miocene) crop out in the footwall. The hanging wall anticline axis trends N–S, like the main thrust plane and like the folds at outcrop scale in the hanging wall. In the analysed outcrop, the relationship between bedding and thrust plane is hanging-wall flat and footwall ramp (sensu Butler, 1983). The cut-off angle in the footwall is about 30–40°.

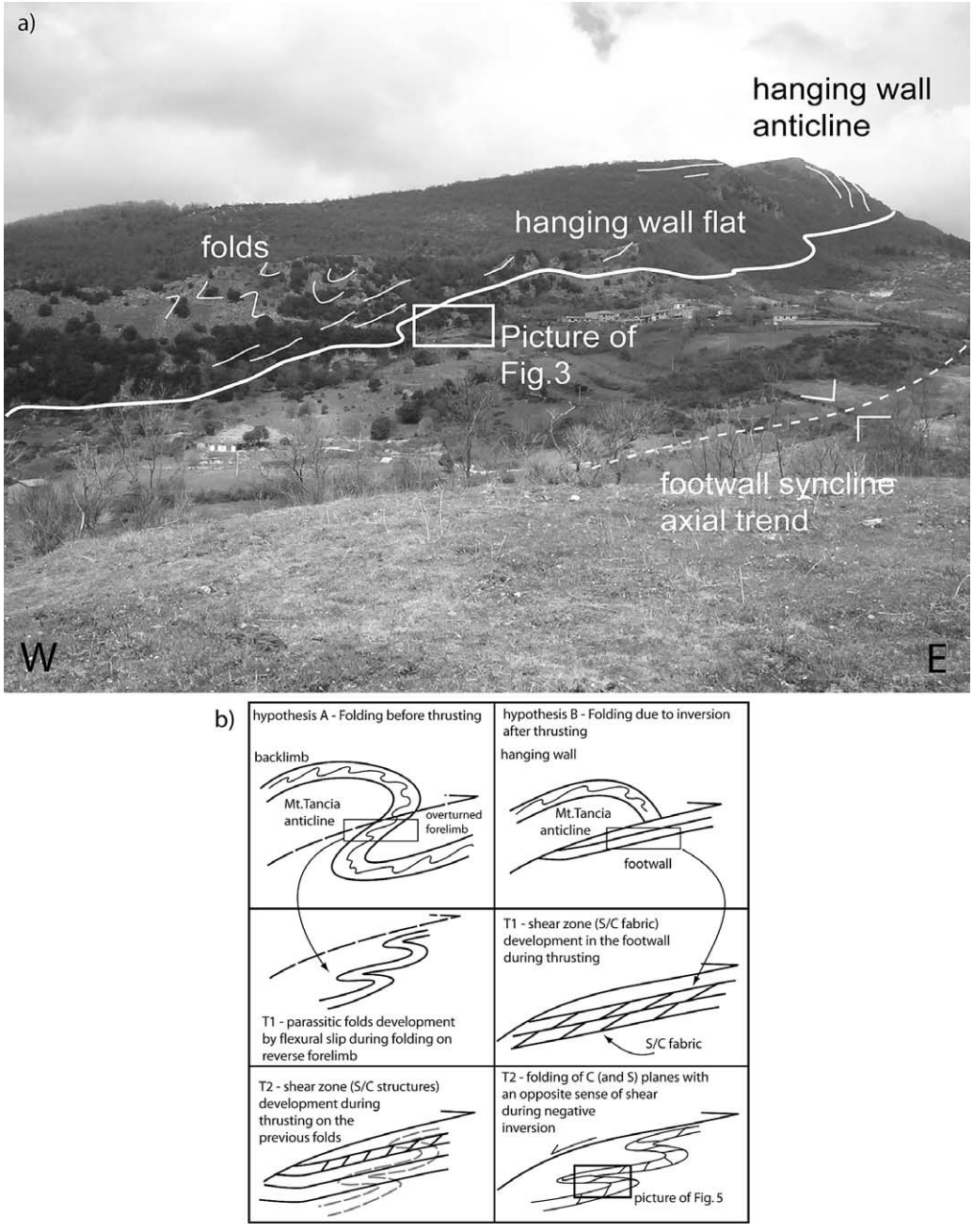

Fig. 2. (a) Mt. Tancia structure. View from south. (b) Two hypotheses to explain the occurrence of folds in the shear zone. See text for discussion.

On the main plane, kinematic indicators, consisting of striations and grooves, indicate a top-to-E–NE sense of transport of the thrust's sheet. The overall geometry defines a transpressional thrust front with a dextral component of shear. At the outcrop scale, the hanging-wall of Mt. Tancia's thrust is offset by an extensional conjugate system, which offsets the fault wall southwestward, with a displacement of about 50 cm–1 m. These normal faults have a mean strike of 150°, and dip of 70–80° southwestward (Fig. 3a).

3. Mt. Tancia's shear zone

The shear zone, about 200 m thick, develops in the marls of the footwall, which consists of a geometrically organized fault rock, ranging from crushed breccias to microbreccias (Sibson, 1977) (Fig. 3). The concentration of deformed rock in the footwall suggests the presence of overpressured fluids in this level (Travè et al., 1998). A detailed structural mapping of the tectonites led to the identification of a complex combination of structures which highlighted opposite sense of shear: although the reverse stratigraphic offset (top-to-NE) of the thrust plane is still conserved, the analysis of the fabric closer to the main plane strongly suggests normal kinematic (top-to-SW). According to the proposed evolution models, the footwall of the main plane, consisting of the marls of the Scaglia Variegata Formation, could represent alternatively the overturned forelimb of Mt. Tancia's thrust hanging wall anticline or the footwall sequence (Fig. 2b). Both hypotheses have been evaluated: in the first one, the top-to-SW sense of shear could represent flexural slip deformation in the forelimb during folding; otherwise, the observed overprinting of a top-to-SW sense of shear on a clearly previous top-to-NE shear zone could indicate the occurrence of structural inversion.

Based on the observed combinations of fabric elements, the shear zone has been divided into three parts, starting from the undeformed rock to the main contact: (i) a lower zone (Z1), (ii) a transitional zone (Z2) and (iii) an upper zone (Z3), closer to the main contact (Figs. 3 and 4).

3.1. The lower zone (Z1)

The Z1 (lower zone) has a thickness of about 50 m (Figs. 3 and 4); at the bottom it gradually changes into undeformed rocks. The pervasive fabric, illustrated in Figs. 3 and 4, is organized into two regular sets of planes: (i) low angle slip surfaces (C-planes) parallel to the fault wall (about 140°/20° SW), with calcite fibres indicating a reverse sense of shear (top-to-NE) and (ii) dissolution cleavage planes 'S' (150°/50° SW). The S surfaces are curved and never displace C surfaces. They are typically confined between two C-planes, forming with an angle of about 30–40°. The more S-planes that were examined, the clearer it became that shear had not occurred on any of them but they showed rough surfaces where dissolution processes largely occurred. Locally, the S-planes form an angle of around 70° with the C-planes and are filled by extensional calcite veins, well observable at outcrop scale. The intersection between S- and C-planes (L1) is normal or at high angle with the fibrous calcite on the C-planes. The C-planes are usually parallel with each other and the spacing between them increases, moving towards the main thrust plane. Moving forward from the main contact, the C-planes are rare or absent and a pervasive fabric of S surfaces (dissolution cleavage) is largely observable.

3.2. The intermediate zone (Z2)

The Z2 zone has a thickness of about 100 m (Figs. 3 and 4). The main fabric, as described for the lower zone, comprises of C-planes and pervasive foliation (S-planes). Moving towards the main contact, the angle between S- and C-planes decreases progressively to a value of 20–10°, whereas the number of S-planes showing fibrous calcite increases. The S-planes were clearly re-worked as shear planes during progressive deformation, as it can be inferred by the superimposition of small and localized fibrous calcite on the already dissolved surfaces. The activation of the S surfaces is likely due to the progressive reduction of the angle with the C-planes, which places them in a more favourable orientation for shear (Berthè et al., 1979; Labaume et al., 1991). The resulting fabric is an irregular and anastomozing foliation, F1, which is largely affected by centimetre-scale folds (Figs. 4 and 5). The axial planes have a mean strike of about 120° and dip of about 10° northeastward. Folds clearly indicate a southwestward sense of shear (top-to-SW), which is inconsistent with the one indicated by the fabric of Z1, and also by the folded S–C fabric itself. The relative chronology of deformation can be reconstructed here because folds (scale from a few millimetres to 10 cm) affect a previously organized S–C fabric, clearly recognizable from ancient S-planes joined to the C folded surfaces. These S-planes, in fact, cannot be confused with axial plane cleavage because they maintain the same sense of shear on both limbs of the fold, as shown on Fig. 5.

3.3. The upper zone (Z3)

The Z3 (upper) zone is about 50 m thick, immediately below the main contact (Figs. 3 and 4). It consists of marls and clays of the Scaglia Variegata Formation (Eocene). The pervasive fabric shows mainly planar structures oriented sub-parallel to the upper fault wall, consisting of sub-parallel S- and C-planes spaced around 5 mm or less. These planes define the F1 foliation, as described in the Z2, which is intensely folded with axial planes striking 150 or 310°, and dipping northeastward.

In the uppermost 4 m, closer to the fault wall, a new set of shear planes can be observed. The new C-planes have a mean strike of 150° and dip of 20° SW with fibrous calcite indicating a southwestern sense of shear. These new C-planes separate bands made of portions of the ancient shear zones. Inside each band a disrupted fabric, consisting of the foliation F1 dipping 40° northeastward with a mean strike of 140°, is recognizable. Planes of F1 foliation include different sub-parallel surfaces, consisting of shear planes, with fibrous calcite indicating a top-to-NE sense of shear (ancient S–C planes) and dissolution

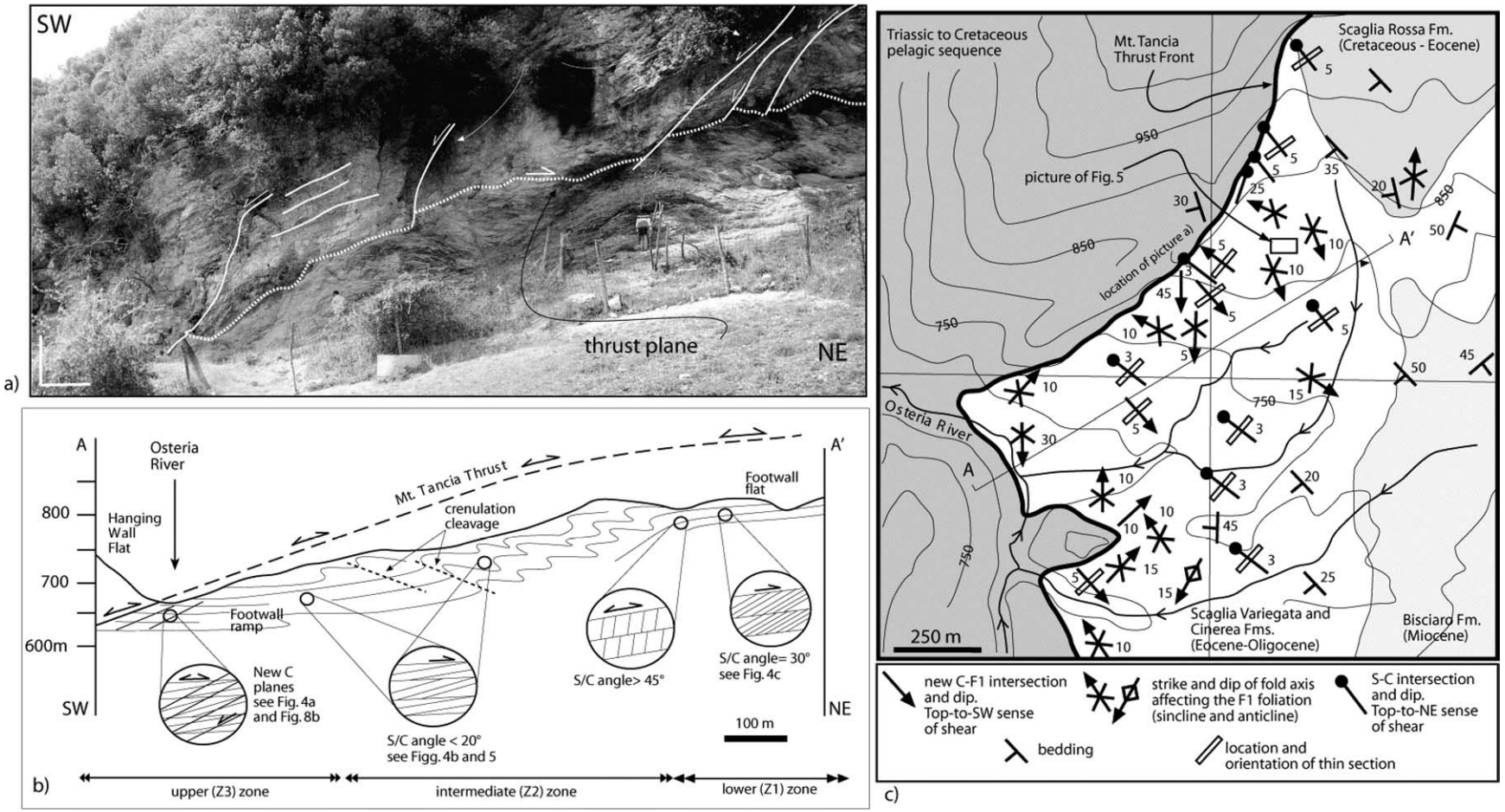

Fig. 3. The Mt. Tancia thrust zone. (a) View of thrust plane from south. Note the hanging wall flat and the footwall ramp relationships. (b) Cross-section of the shear zone where Z1, Z2 and Z3 are located. (c) Structural map of tectonites in the footwall of the thrust.

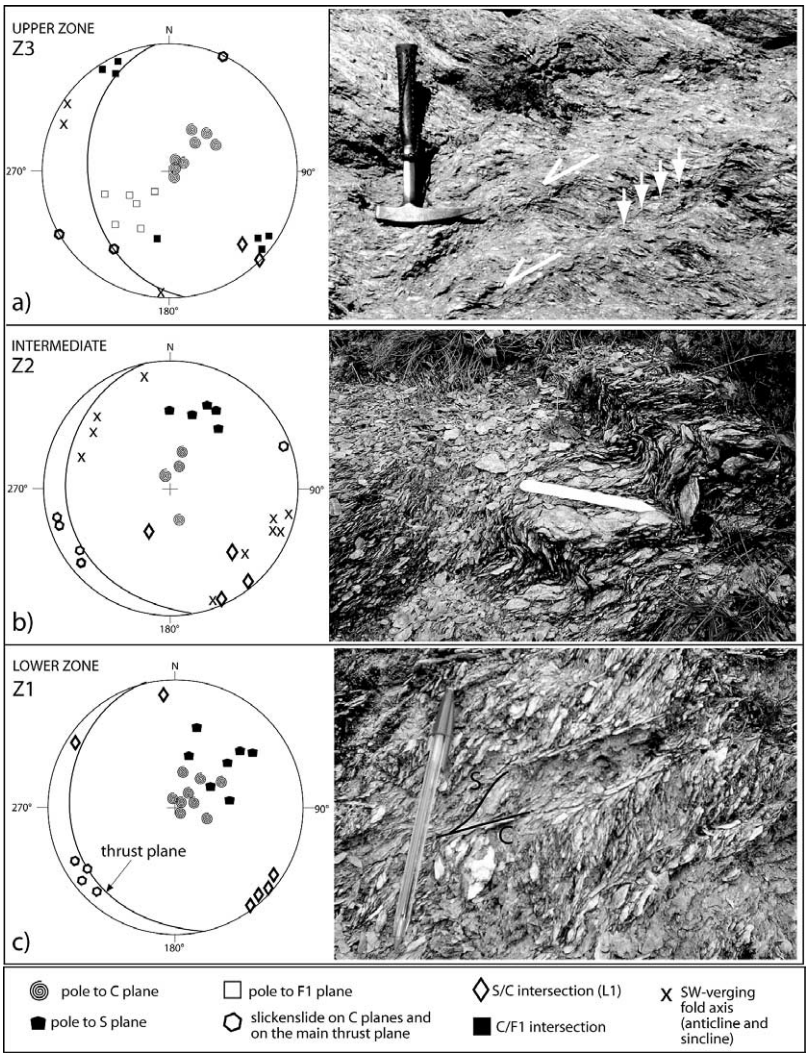

Fig. 4. Progressive deformation of the Mt. Tancia shear zone and projection of the main measured structural elements (Schmidt projection, lower hemisphere).

planes (S-planes) (Figs. 3 and 4). The latter form an angle of 40° with the new C-planes and seem to overprint the ancient S–C fabric; they cross the foliation F1 and, across them, it is possible to observe the occurrence of disrupted and dissolved extensional calcite veins.

Occurrence of extensional structures inside a shear zone is largely documented and discussed (Platt and Vissers, 1980; Koopman, 1983; Platt, 1984; Calamita, 1991; Cowan and Brandon, 1994; Blenkinsop and Treloar, 1995; Cladouhos, 1999a,b and references therein). These planes, called antithetic and synthetic Riedel shear, have been interpreted to be Coulomb slip surfaces. They form, respectively, at 15 and 75° from the main shear surface (Cladouhos, 1999a,b and references therein). The new C-planes observed in the upper part of Z3 shear zone of Mt. Tancia's thrust, although showing extensional kinematics, have not been interpreted as Riedel planes based on the following observations.

The new C-planes are strongly localized in this part of the shear zone, instead of being distributed all over the deformed fault rocks. Variable density of Riedel shear occurrence inside a brittle shear zone is explained by Cladouhos (1999a,b and references therein) as due to different contributions of components of deformation. In the case of absence of Riedel planes inside the shear zone, Cladouhos demonstrated that the main component of deformation can be particulate flow that produces a foliation parallel to the shear planes, which is the predominant fabric of the shear zone. Therefore, in the case of the upper part of the Z3 zone, where F1 foliation is well developed, high angle shear planes largely occur (where they should be either absent or reduced) while they are absent in the other part of the shear zone, where instead Riedel planes (synthetic and antithetic Riedel shear) should occur in order to accommodate strain.

New C-planes occur in shear zones where F1 foliation, instead of parallel, assumes an angular relationship (about 40°) with the main thrust plane, which varies its dip angle passing from a flat to a ramp geometry (Fig. 2). The new C-planes are sub-parallel to the main thrust plane (at high angle with the ancient F1 foliation) and dip southwestward, which means that F1 foliation likely developed before the onset of new C-planes. Moreover, they have both strike and dip in the opposite direction with respect to the ones theoretically predicted for

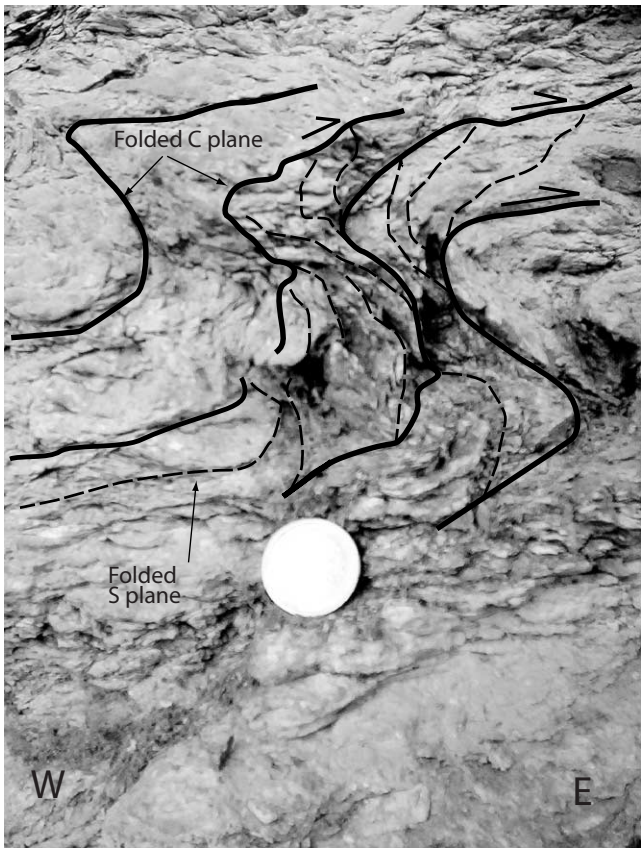

Fig. 5. Folded C-planes. See text for discussion.

Riedel shear planes; the fabric is completely re-arranged around these new structures: a new set of dissolution cleavage planes (new S-planes) overprinting F1 foliation can be recognized.

4. Microstructural observations

Several thin sections were collected from Mt. Tancia's shear zone. Each sample was oriented in the field; back in the laboratory, they were reduced and cut to obtain sections normal to the S/C planes intersection and parallel to the fibrous calcite on the C planes. The orientation of the section with respect to the C-planes was marked for each sample on the thin section by reorienting the sample in the laboratory using a sand box. The locations of samples for thin sections are shown in Fig. 3. The microstructural features of all the samples consist of a discontinuous (Z1) to pervasive (Z3) fabric, comprising dissolution surfaces (stylolite) and extensional calcite veins. For the sections from Z1, the main problem has been to obtain an area comprising all of the structures visible at outcrop scale: lithons among S- and C-planes were usually too large and the surface of thin section covered just a part of the lithon. Thin sections from Z1 illustrate a discontinuous fabric, with dissolution surfaces (stylolites) and veins isolating relatively large undeformed portions of rock, with a fairly simple geometry. Thin sections from Z2 and Z3, instead, show a more pervasive fabric consisting of the same features (veins and dissolution surfaces) with a higher density and reduced spacing (Fig. 6).

Different types of veins are recognizable, likely associated with different events of crystallization:

Type I includes very thin, irregular and long veins, sub-parallel to each other. Vein fill generally appears as microsparite made of calcite crystals the size of a few tens of a micron (20–40 μm). Locally these veins form a network intersecting each other at different angles. Type I veins are present in all the thin sections analysed and seem to represent the first event of crystallization based on the cross-cutting relationship with the other features (Fig. 6a and b). Vein network development has been described during events of overpressure inside brittle shear zones, which can occur several times before the onset of the pressure-solution process, and they are considered a feature associated with the deformation of non-fully consolidated sediments (Labaume et al., 1997; Travè et al., 1998; Vannucchi and Maltman, 2000).

Type II includes extensional veins at an angle of 50–70° with the shear C-planes (Fig. 6a and c). These veins show an extremely variable thickness, they are quite short and often bifurcated at their edges. The vein fill consists of calcite crystals (200–600 μm), filled by several events of crystallization. In the syntaxial veins, the first generation of growth is well recognizable: the crystals are parallel with each other and normal to the wall vein. Sometimes, the central area is filled by foam structures (calcite crystals with a mosaic feature) (Fig. 6c), with smaller grains and two or more median lines. Diffuse pressure-solution phenomena occur along vein boundaries as well as along crystal rims. Most veins are cut by dissolution surfaces consuming part of the vein, whereas others propagate across the dissolution cleavage without being offset; in this case, just a reduction of the grain size and a re-organization of the vein fill are visible. These cross-cutting relationships indicate a progressive evolution of shear-driven dilatation and collapse, comprising repeated events of dissolution and dilatation (with opening and filling of veins).

Type III are irregular patches, located at the intersection between differently oriented dissolution cleavages and occur in all the thin sections examined (Fig. 6a, d and e). In these patches, a geometric relationship with the vein wall is not recognizable and calcite crystals show a mosaic or foam organization. Moreover the internal deformation of each crystal does not differ from the ones in the veins described before. In a first analysis, this feature has been associated with larger dislocation of pre-existing veins. This is evident in some cases where, along the boundaries of the veins, elongated crystals normal to the vein wall are preserved.

Type IV are very small shear veins along dissolution surfaces, oriented parallel to the C-planes. They are visible in thin sections from Z2 and Z1 and can be interpreted as the reactivation of rotated S-planes inside the shear zone (Berthè et al., 1979).

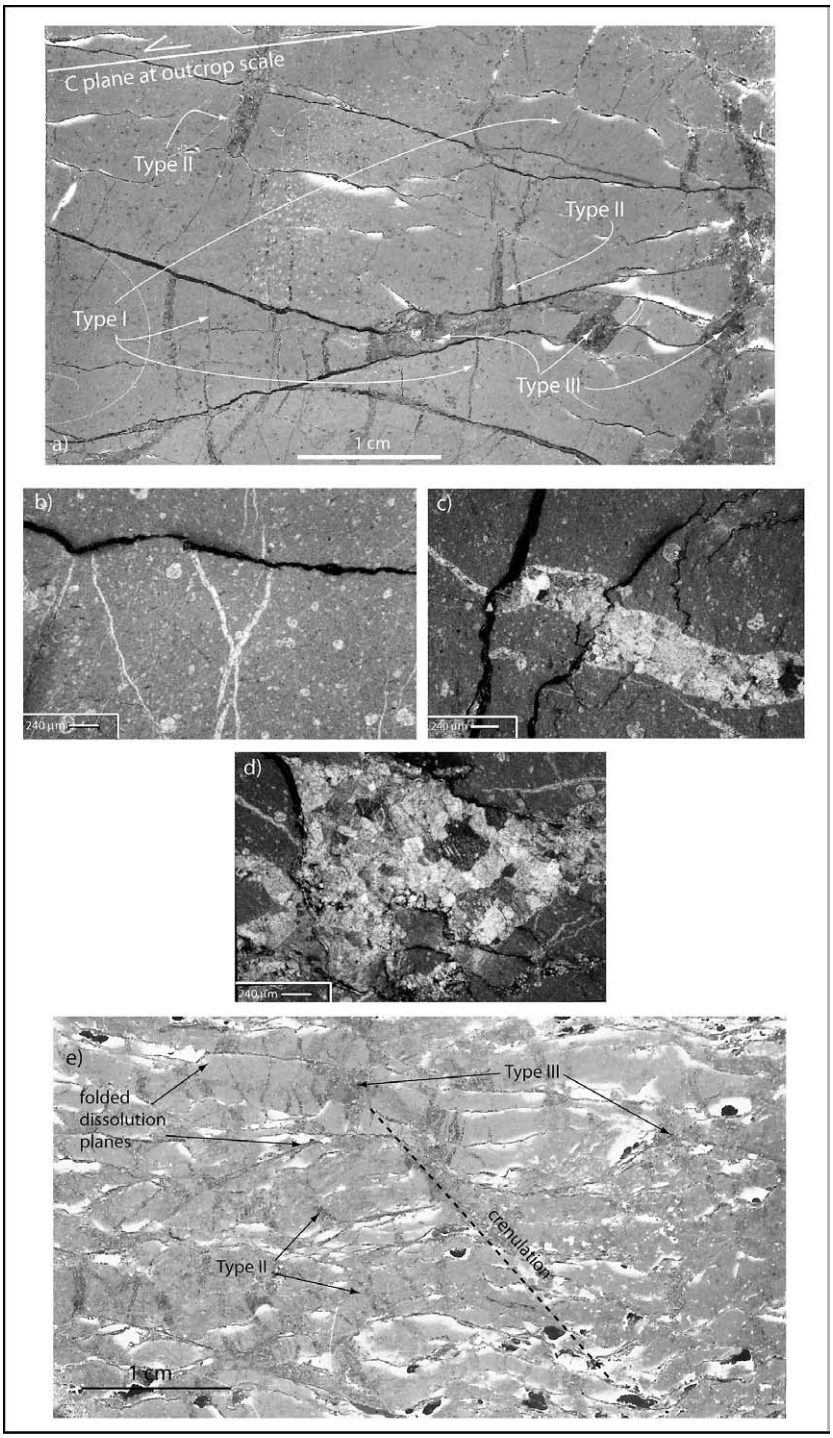

Fig. 6. Thin sections from Mt. Tancia shear zone. (a) Z1 zone. The relationship among different types of veins can be observed. (b) Veins of type I. (c) Veins of type II. (d) Veins of type III. (e) Thin section from the upper part of Z3 zone. The folded vein/dissolution planes form a crenulation feature in the right part of the thin section, oriented compatible to the normal shear sense of reactivation. The fault wall is parallel to the top of the photograph and the sense of inversion is toward the left.

4.1. Evidence of structural reactivation within the Z1 zone

In thin sections from Z1, dissolution planes are closely spaced, anastomozed, sub-parallel to the fault wall and largely folded (Fig. 6e). The folds are open, asymmetric and have a wavelength of about 50 mm. Axial planes dip northeastward. Spacing of dissolution surfaces and orientation of the axial planes tend to form crenulations planes, which are themselves sites of dissolution. Crenulation is oriented at about 50° with respect to fault wall (C-planes). Type IV veins, quite parallel to dissolution cleavage, are folded with it. Veins of type II, occupying nearly half of the fault rock, are repeatedly disrupted by dissolution cleavage and are passively rotated during folding, as visible by the ‘fan’ distribution of veins around

the hinge of the folds. The folding process could be triggered by mechanical slip along crystal boundaries, as well as being visible at the hinge of the folded veins. The fill consists of calcite crystals arranged with a foam structure (Type III).

4.2. Fluid flow and stress regime

The wide occurrence of veins in Mt. Tancia's shear zone suggests that the plausible deformation mechanisms were hydrofracturing and pressure-solution. Many authors have described how these two mechanisms can act inside a shear zone as a function of stress regime, magnitude of differential stress, progressive stages of sediments' diagenesis and rises and drops of fluid pressure (Cello and Nur, 1988; Labaume et al., 1991; Moore et al., 1995; Caine and Forster, 1999; Vannucchi, 2001 and references therein). Extensional veins and generations of mosaic calcite crystals like the types II and III observed in the Mt. Tancia's shear zone necessitate high fluid pressure. On the other hand, the quite constant orientation of the repeated generation of type II veins observed in the thin sections (about 50–70° with C-planes) suggest that the stress regime remained quite constant and the veins orientation with respect to C-planes indicates that $\sigma 1$ orientation was kept constant during the entire mineralization process. The mosaic morphology of the calcite crystals developed under these conditions, when the fluid pressure approaches the $\sigma 1$ value, the hydrostatic stress regime is reached and fluids could freely crystallise in opened fractures; after crystallisation, when instead fluid pressure decreased, a direction of easy opening, parallel to $\sigma 3$, was again clearly defined.

5. The twinning of calcite

The calcite crystals in the thin section show a twinning deformation. This deformation mechanism in calcite becomes important starting from a very low grade of deformation and can be used as temperature, strain and possibly stress indicators (Burkhard, 1993 and references therein; Gonzales-Casado and Garzia-Cuevas, 1999; Nemcok et al., 1999; Fry, 2001; Ferrill et al., 2004). Generally, twinning occurs along three e-planes inclined towards the c-axis and it is initiated at very low critical resolved shear stress (2–12 MPa; Turner et al., 1954; Burkhard, 1993). It has also been suggested that it might depend on differential stress and calibrated with respect to its variation (Rowe and Rutter, 1990). In any case, the amount of strain accommodated by twinning is generally small and usually pressure/solution and grain boundary migration at grain boundaries are also present. A morphological analysis at the optical microscope of twins observed in the calcite crystals of veins has been performed, based on the classification proposed by Burkhard (1993) (Fig. 7). This classification has been well constrained by several independent geothermometers in the Helvetic Nappes in Switzerland and others places, such as the Appalchians (Groshong, 1988; Evans and Dunne, 1991). It is based on the notion that the morphological aspect of twinning (thickness, geometry of twin at grain boundary, twin–twin relationship, etc.) is mainly a function of temperature, even if the reason for this relationship is not completely understood (Burkhard, 1993). Most of the crystals observed in veins from Mt. Tancia's shear zone show one or two sets per grain; only in a few cases were there three sets present. Generally the thickness of twins is grater than 5 μm (10–20 μm). They are straight and show a slight lense shape. In some cases the grain boundary dislocated by the twin lamellae is still recognizable. The described features correspond to type II of the Burkhard classification (Fig. 7b and c). Very few cases belonged to type III with curved and thick twin lamellae, twin in twin (rational) and crystals completely twinned (Fig. 7a, b and e). The range of temperature defined by the morphology of twin lamellae (type II) is between 150 and 300 °C. The interpretation is in agreement with the development of a shear zone in areas characterized by a non-metamorphic regime, with a reduced cover and at a relatively shallow level. The occurrence of the type III can also be explained as the result of a peak of stress concentrated in the shear zone, possibly associated with crack and seal mechanism (Sibson, 1990) and small earthquakes.

6. Discussion

There is a widespread acceptance of the idea that simple shear is prevalent in shear zones. This model, generally applied to ductile shear zones (Berthè et al., 1979; Platt and Vissers, 1980; Ramsay and Huber, 1983, 1987; Lister and Snoke, 1984; Platt, 1984) has been extended to brittle and brittle–ductile fault rocks (Chester and Logan, 1987; Labaume et al., 1991; Cowan and Brandon, 1994; Cladouhos, 1999a,b). At the same time, the possibility to describe deformation as a combination of different deformation models acting together inside the shear zone was explored, taking into account problems of scale, of continuous–discontinuous nature of deformation, of volume variation and of rotation rate of crystal axis and rigid clasts (Berthè et al., 1979; Lister and Williams, 1979; Passchier and Simpson, 1986; Blenkinsop and Treloar, 1995; Cladouhos, 1999b).

In the case of Mt. Tancia's shear zone, the observed S dissolution planes are assumed to lie parallel to the XY-plane of the local finite ellipsoid, based on several pieces of evidence: (i) the S dissolution cleavage is quite continuous from Z1 to the undeformed rock around the shear zone, with the same geometric characters; (ii) slip did not occur on S-planes; (iii) L1 intersection is quite perpendicular to shear indicators (fibrous calcite) on C-planes, and parallel to kinematics indicators on the main plane. A progressive reduction of the angle between S- and C-planes and an increase in C-planes density occur from the undeformed zone towards the main plane at the outcrop scale; S-planes are re-used as shear planes just in the upper part (Z3) of the shear zone (closer to the main thrust plane). This evidence suggests that a deformation developed with the S-planes parallel to the XY-plane of local strain ellipsoid in domains between discrete shear surfaces (C-planes). Both rotation of S surfaces and slip on C surfaces accommodate the total strain at outcrop scale (Blenkinsop and Treloar, 1995). Explaining this geometrical organization in terms of simple shear model implies the consideration of the C

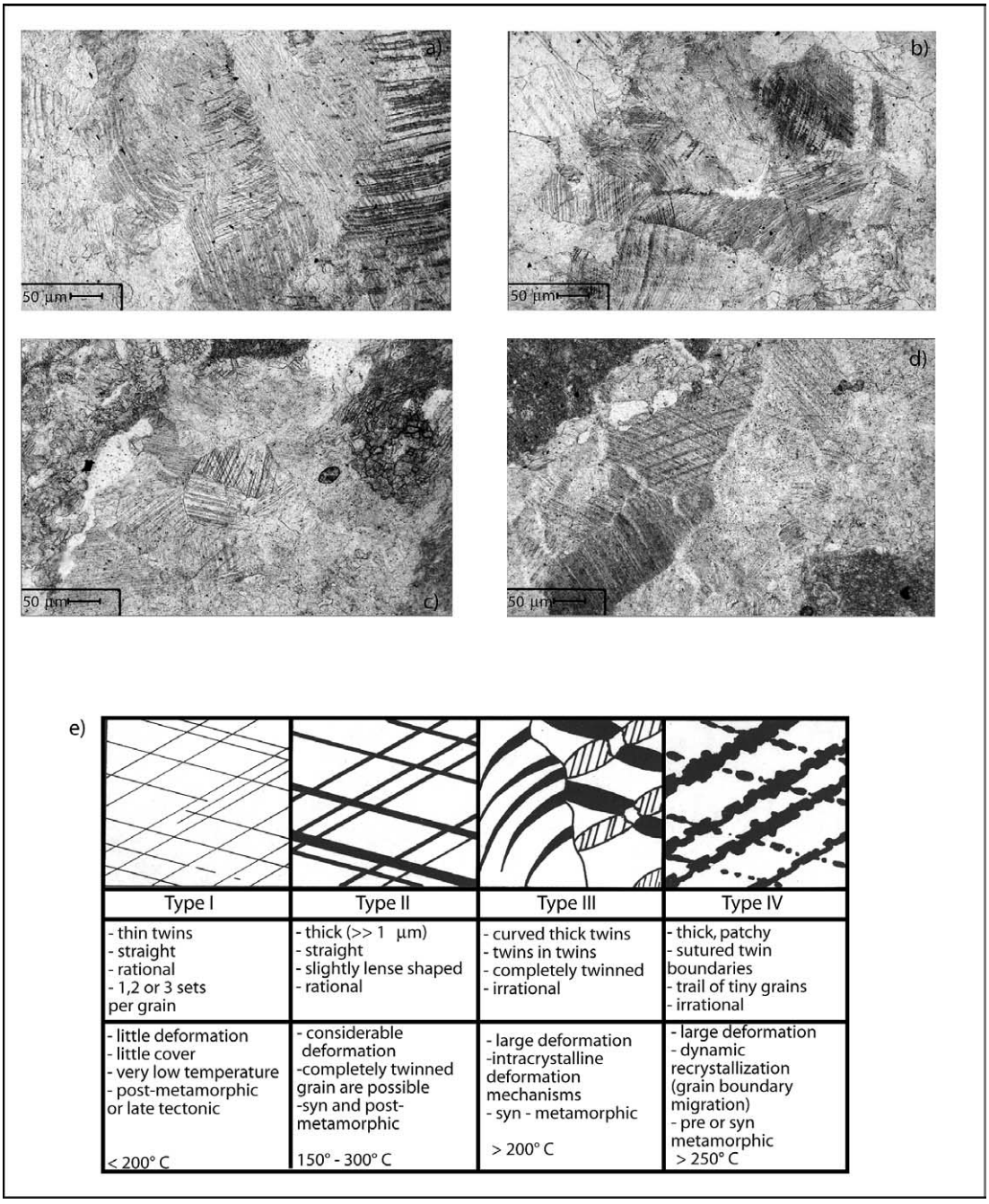

Type I	Type II	Type III	Type IV
- thin twins - straight - rational - 1,2 or 3 sets per grain	- thick (>> 1 µm) - straight - slightly lense shaped - rational	- curved thick twins - twins in twins - completely twinned - irrational	- thick, patchy - sutured twin boundaries - trail of tiny grains - irrational
- little deformation - little cover - very low temperature - post-metamorphic or late tectonic < 200° C	- considerable deformation -completely twinned grain are possible -syn and post-metamorphic 150° - 300° C	- large deformation -intracrystalline deformation mechanisms - syn - metamorphic > 200° C	- large deformation - dynamic recrystallization (grain boundary migration) - pre or syn metamorphic > 250° C

Fig. 7. Example of twin types from the shear zone of Mt. Tancia's thrust. Type II are shown in (b) and (c), whereas types II and III are present in (a), (b) and (e). All the twin lamellae are thicker than 1 µm and two or tree sets per grain are present; (e) classification of twin deformation features, from Burkhard (1993), modified.

surface as a zone of concentration of shear but essentially as a continuous at the outcrop scale, in order to guide rotation of S-planes as XY-planes. In the field, C-planes are defined by several generations of fibrous calcites (Figs. 4 and 5), which grew progressively during slip along C surfaces, even if it is most likely that this happened in time, through more than one event. In this case, during the growing of fibrous calcite, C-planes worked as continuous shear planes and a connection between slip along C surfaces and rotation of S-planes can be established.

On the other hand, deformation observed at thin section scale seems to be better described with a different approach. As already described, veins show several crystallization events, due to the interaction between fluid pressure and differential stress variations, but the orientation of veins keeps quite constant, suggesting that no rotation of strain axes took place during deformation. Veins opened approximately normal to the direction of maximum instantaneous lengthening; during deformation they become wider and propagated laterally outward parallel to the instantaneous shortening axis. This suggests the occurrence of components of coaxial deformation inside the shear zone. Some authors point out that, although the bulk deformation in a shear zone may approximate to simple shear, smaller volumes inside the shear zone can follow

a coaxial deformation path (Lister and Williams, 1979). If this is the case, whereas the outcrop organization suggests a progressive simple shear model, the deformation of veins may have remained coaxial; it is the pulses of high pore pressure that snapshot an instantaneous strain during the increasing of differential stress at veins scale that make the non-passive behaviour possible.

6.1. Simplified 2D analysis of structural inversion

Even the geometry observed in Z1, and interpreted as the result of a structural inversion in a normal sense of shear, shows numerous analogies with inverted ductile shear zones. Evidence of structural inversion consists of superimposition of structures inside the shear zone that are incompatible with the previous recognized sense of shear. This methodology has been adopted by several authors (Holdsworth, 1994; Beeson et al., 1995; Butler et al., 1995; Wennberg, 1996; Worley and Wilson, 1996; Nyman, 1999; Maruyama and Lin, 2004) who pointed out how new structures are superimposed on the older ones, and their orientation depends also on anisotropies generated by the older fabrics.

A simplified 2D analysis has been performed using a PC drawing program, with the aim of better describing the development of these new fabric elements inside the Mt. Tancia's shear zone (Fig. 8a). Although the Mt. Tancia's shear zone is likely the results of different components of deformation, this model allows the description of the behaviour of S- and C-planes, assumed to be passive markers during structural inversion. The geometry of lines rotation is controlled by the relation:

$$\cot \alpha' = \cot \alpha - \gamma \tag{1}$$

where the angle between α and α' is defined as line rotation w (Ramsay and Huber, 1987) and γ is the shear strain.

The starting configuration is composed of a simple square with a marker line inclined by 45° (S-plane). For a top-to-NE sense of shear (dextral in Fig. 8a), the passive marker is located at 45° with the shear plane at the beginning of deformation. As it is predicted, at higher values of shear strain the angle

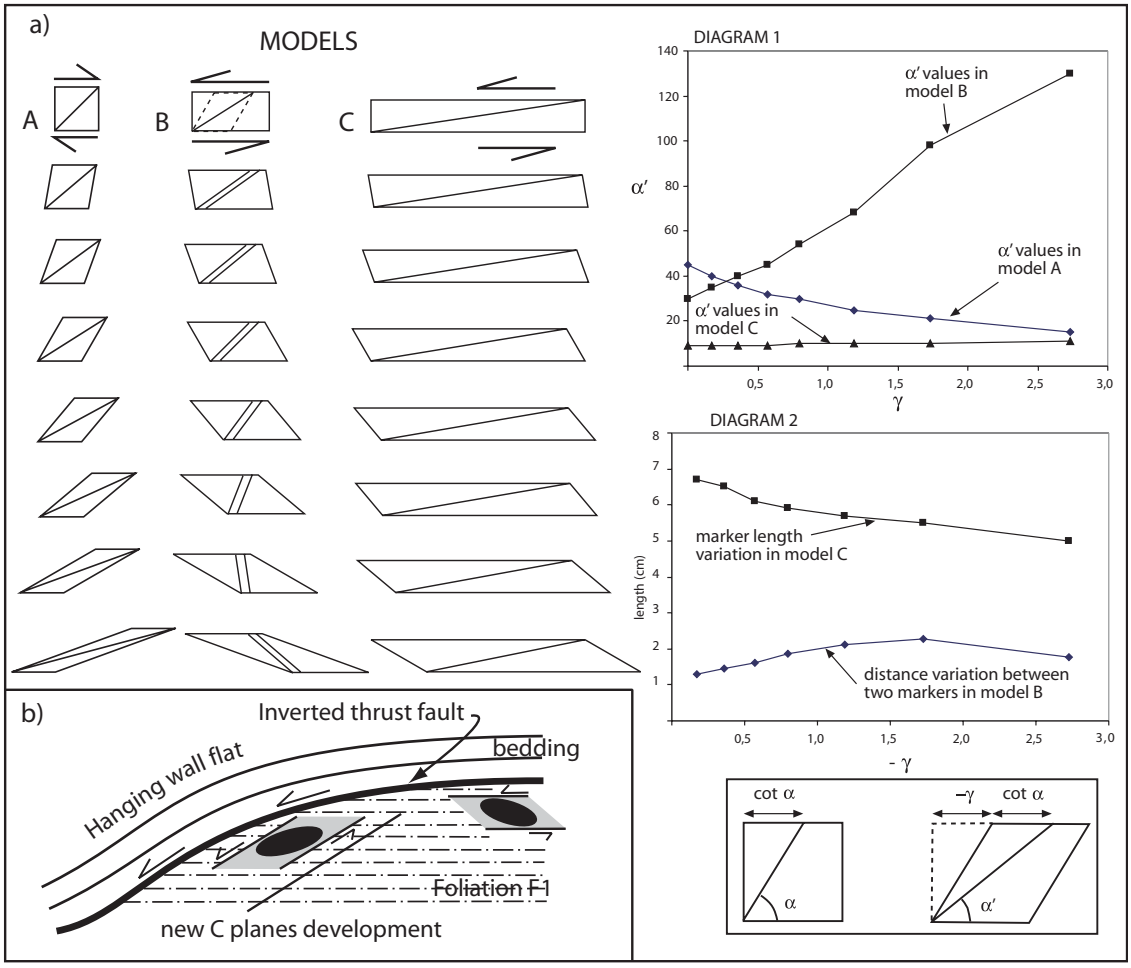

Fig. 8. (a) Simplified 2D analysis using a 2D drawing program (Models A, B and C). The inferred rotation is every 10°. The line rotation in a progressive simple shear are shown during the top-to-NE sense of shear (A) and during inversion acting in the lower zone (B) and in the upper zone (C). Relationships between shear strain and α' for each model are shown in diagram 1, whereas in diagram 2 the length variation of marker in model C and the distance variation between the two markers of model B are shown. The cartoon represents the relationship of line rotation and shear strain in simple shear (from Ramsay and Huber (1983), modified). (b) The sketch describes the configuration of strain ellipsoid inferred during inversion of the main thrust fault in the Z3 zone. See text for discussion.

between the S- and C-planes decreases from 45 to 20° during the progressive rotation, as can be observed in the Mt. Tancia's shear zone moving towards the fault wall (Fig. 8a, model A, diagram 1).

Reactivation in the opposite sense of shear determines a rotation of the previous structures in the opposite sense (models B and C in Fig. 8a). A top-to-SW rotation (sinistral in Fig. 8a) has been imposed on the model, starting from two different configurations. The first one is related to Z1 (Fig. 8a, model B) where the angle between the S- and C-planes is about 30° and the second one (model C in Fig. 8a) is representative of F1 foliation in the Z2–Z3 part of the shear zone (angle of 10°). For the first model, the imposed opposite sense of shear induces a local extension normal to S-planes: the distance between the two markers in model B increases during sinistral rotation and that is in agreement with the occurrence of extensional veins filling ancient S-planes at outcrop scale in the Z1 part of the shear zone (Fig. 8a, diagram 2).

In model C the starting angle of passive marker is 10°. It simulates the S/C planes (defined above as F1 foliation) associated with top-to-NE kinematics. As shown in Fig. 8a (model C, diagram 2), for low values of shear, the configuration of S/C planes maintains a geometry that indicates a top-to-NE sense of shear and, at the same time, a length reduction, but substantially no rotation of the passive marker occurs. This indicates that the marker is oriented in the contractional field of the instantaneous strain ellipse generated by the opposite sense of shear and it underwent contraction instead of rotation. Therefore the development of folds in Mt. Tancia's shear zone can be explained considering the orientation of F1, which, when the opposite sense of shear is imposed, is oriented in the contractional field of the local strain ellipse (Z2 of Mt. Tancia's shear zone). At thin section scale, the orientation of crenulation planes is parallel to the XY-plane generated by the opposite sense of shear.

Closer to the outcropping thrust plane the configuration of the strain ellipsoid during structural reactivation varies again. Here in fact F1 foliation shows a footwall ramp relationship with respect to the main fault plane (Fig. 8b), with an angle of about 40°. With this starting configuration, F1 foliation is oriented quite parallel to the maximum elongation axis of the instantaneous strain ellipse generated by the opposite sense of shear. In this condition, new C-planes dipping SW were generated, whereas foliation F1 was re-activated as dissolution cleavage (Fig. 8b). The interaction between F1 orientation with respect to the main fault plane, and the imposed sense of movement of the latter, can explain the space distribution of the new C-planes dipping SW, which are concentrated closer at the main contact.

7. Conclusion

The analysed fault rocks associated with Mt. Tancia's thrust, document a structural (sensu Holdsworth et al., 1997) negative inversion of a thrust fault, from the core (closer to wall fault) towards the more external part (Figs. 3–5). Evidence of a negative inversion has been documented by the geometric and kinematic properties of the fabric exposed within an about 200-m-thick shear zone. Two kinds of elements are here recognizable: a fabric indicating a top-to-NE (reverse) tectonic transport and a fabric indicating an opposite (top-to-SW) sense of shear that is superimposed on the previous one. The analysed shear zone fabrics include dissolution surfaces (S-planes) and shear planes (C-planes), whereas the main deformation mechanism is pressure solution. During shear zone evolution, S- and C-planes develop simultaneously, while slip occurring on C-planes induces a rotation of S-planes, probably parallel to the XY-plane of local strain ellipsoid, at least during the growth of fibrous calcite events. This mechanism allows the deformation to be described using a simple shear model. At microscope scale, the configuration of calcite veins suggests that a component of coaxial deformation acted in the shear zone at that scale, whereas reactivation generated folding and crenulation cleavages compatible with a top-to-SW sense of shear. The overall evolution of the shear zone occurred in the so-called twin regime (Burkhard, 1993) at temperatures around 150–200 °C.

Acknowledgements

I would like to thank Dott.ssa Patrizia Costa Pisani and Sofia Mariano for the kind help in the sampling of the shear zone. Many thanks to Professors Carlo Doglioni, Goffredo Mariotti and Eugenio Carminati for the useful discussions both in the field and in laboratory. The paper greatly benefited from the constructive reviews by the Editor, T.G. Blenkinsop, and the two referees, G. Cello and C. Doglioni.

References

Beeson, J., Harris, L.B., Delor, C.P., 1995. Structure of the western Albany Mobile Belt (southwestern Australia): evidence of overprinting by Neoproterozoic shear zones of the Darling Mobile Belt. Precambrian Research 75, 47–63.

Berthè, D., Choukroune, P., Jegouzo, P., 1979. Orthogneiss, mylonite and non coaxial deformation of granites: the example of the South Armorican Shear zone. Journal of Structural Geology 1, 31–42.

Blenkinsop, T.G., Treloar, P.J., 1995. Geometry classification and kinematics of S–C and S–C′ fabrics in the Mushandiche area, Zimbabwe. Journal of Structural Geology 17, 397–408.

Burkhard, M., 1993. Calcite-twins, their geometry, appearance and significance as stress-strain markers and indicator of tectonic regime: a review. Journal of Structural Geology 15, 351–368.

Butler, C.A., Holdsworth, R.E., Strachan, R.A., 1995. Evidence for Caledonian sinistral strike-slip motion and associated fault zone weakening, Outer Hebrides Fault Zone, NW Scotland. Journal of the Geological Society, London 152, 743–746.

Butler, R.W.H., 1983. Thrust sequences. Journal Geological Society of London 144, 619–634.

Caine, J.S., Forster, C.B., 1999. Fault zone architecture and fluid flow: insights from field data and numerical modeling. In: Haneburg, W.C., Mozley, P.S., Moore, J.S., Goodwin, L.B. (Eds.), Faults and Subsurface Fluid Flow in the Shallow Crust. American Geophysical Union Monograph 113, pp. 101–127.

Calamita, F., 1991. Extensional mesostructures in thrust shear zones: examples from the Umbro-Marchean Apennines. Bollettino Società Geologica Italiana 110, 649–660.

Cavinato, G.P., Salvini, F., Tozzi, M., 1986. Evoluzione strutturale del settore centrale della Linea Olevano-Antrodoco. Memorie Società Geologica Italiana 35, 591–601.

Cavinato, G.P., Chiaretti, F., Cosentino, D., Serva, L., 1989. Caratteri geologico-strutturali del margine orientale della Conca di Rieti. Bollettino Società Geologica Italiana 108, 207–218.

Cello, G., Nur, A., 1988. A model for the emplacement of thrust systems. Tectonics 7, 261–271.

Chester, F.M., Logan, J.M., 1987. Composite planar fabric of gouge from the Punchbowl Fault, California. Journal of Structural Geology 9, 621–634.

Civitelli, G., Corda, L., Mariotti, G., 1986. Il bacino sabino: (1) fenomeni di risedimentazione nella serie di Osteria Tancia. Bollettino Società Geologica Italiana 105, 41–63.

Cladouhos, T.T., 1999a. A kinematic model for deformation within brittle shear zone. Journal of Structural Geology 21, 437–448.

Cladouhos, T.T., 1999b. Shape preferred orientation of survivor grains in fault gouge. Journal of Structural Geology 21, 419–436.

Cosentino, D., Parotto, M., 1992. La struttura a falde della Sabina (Appennino Centrale). Studi Geologici Camerti, volume speciale 1991/2 CROP 11, 381–387.

Cowan, D.S., Brandon, M.T., 1994. A symmetry-based method for kinematic analysis of large slip brittle fault zone. America Journal of Science 294, 257–306.

Evans, M.A., Dunne, W.M., 1991. Strain factorization and partitioning in the North Mountain thrust sheet, central Appalachians, U.S.A. Journal of Structural Geology 13, 21–35.

Faccenna, C., Nalpas, T., Brun, J.P., Davy, P., 1995. The influence of pre-existing thrust faults geometry in nature and in experiments. Journal of Structural Geology 17, 1139–1149.

Ferrill, A.D., Morris, A.P., Evans, M.A., Burkard, M., Groshong, R.H., Onasch, C.M., 2004. Calcite twin morphology: a low-temperature deformation geothermometer. Journal of Structural Geology 26, 1521–1529.

Fry, N., 2001. Stress space: striated faults, deformation twins, and their constraints on paleostress. Journal of Structural Geology 23, 1–9.

Gonzales-Casado, J.M., Garzia-Cuevas, C., 1999. Calcite twins from microveins as indicator of deformation history. Journal of Structural Geology 21, 875–889.

Groshong, R.H., 1988. Low temperature deformation mechanisms and their interpretation. Bulletin Geological Society of America 85, 1855–1864.

Holdsworth, R.E., 1994. Structural evolution of the Gander-Avalon terrane boundary: a reactivated transpression zone in the NE Newfoundland Appalachians. Journal of Geological Society of London 151, 629–646.

Holdsworth, R.E., Butler, C.A., Roberts, A.M., 1997. The recognition of reactivation during continental deformation. Journal of Geological Society of London 154, 73–78.

Ivins, E.R., Dixon, T.H., Golombek, M.P., 1990. Extensional reactivation of an abandoned thrust: a bound on shallowing in the brittle regime. Journal of Structural Geology 14, 991–998.

Koopman, A., 1983. Detachment tectonics in the Central Apennines, Italy. Geologica Ultraiectina 30, 1–155.

Labaume, P., Berthy, C., Laurent, Ph., 1991. Syn-diagenetic evolution of shear structures in superficial nappes: an example from the Northern Apennines (NW Italy). Journal of Structural Geology 13 (4), 385–398.

Labaume, P., Maltman, A.J., Bolton, A., Teisser, D., Ogawa, Y., Takizawa, S., 1997. Scaly fabrics in sheared clays from the decollement zone of the Barbados Accretionary prism. ODP Leg 156. In: Shipley, T.H., Ogawa, Y., Blum, P., Bhar, J.M. (Eds.), Proceeding of ODP, Scientific Results, Vol. 156, pp. 59–77.

Lister, G.S., Snoke, A.W., 1984. S–C mylonites. Journal of Structural Geology 6 (6), 617–638.

Lister, G.S., Williams, P.F., 1979. Fabric development in shear zones: theoretical controls and observed phenomena. Journal of Structural Geology 1, 283–297.

Malavielle, J., 1987. Kinematics of compressional and extensional ductile shearing deformation in a metamorphic core complex of the North Eastern Basin and Range. Journal of Structural Geology 9, 541–554.

Maruyama, T., Lin, A., 2004. Slip sense inversion on active strike-slip faults in southwest Japan and its implications for Cenozoic tectonics evolution. Tectonophysics 383, 45–70.

Moore, J.C., Shipley, T.H., Goldberg, D., Ogawa, Y., Filice, F., Fisher, A., Jurado, M.J., Moore, G.F., Rabaute, A., Yin, H., Zwart, G., Brückmann, W., Henry, P., Ashi, J., Blum, P., Meyer, A., Housen, B., Kastner, M., Labaume, P., Laier, T., Leitch, E.C., Maltman, A.J., Peacock, S., Steiger, T.H., Tobin, H.J., Underwood, M.B., Xu, Y., Zheng, Y., 1995. Abnormal fluid pressures and fault-zone dilation in the Barbados accretionary prism: evidence from logging while drilling. Geology 23, 605–608.

Nemcok, M., Kovac, D., Lisle, R., 1999. A stress inversion procedure for polyphase calcite twin and fault/slip data sets. Journal of Structural Geology 21, 597–611.

Nyman, M.W., 1999. Fabric reactivation: an example from the Hualapai Mountains, NW Arizona, USA. Journal of Structural Geology 21, 313–321.

Passchier, C.W., Simpson, C., 1986. Porphyroblast systems as kinematics indicators. Journal of Structural Geology 8, 831–843.

Platt, J.P., 1984. Secondary cleavages in ductile shear zones. Journal of Structural Geology 6 (4), 439–442.

Platt, J.P., Vissers, R.L.M., 1980. Extensional structures in anisotropic rocks. Journal of Structural Geology 2, 397–410.

Powell, C.M., Williams, G.D., 1989. The Lewis/Rocky Mountain Trench fault system in the Northwestern Montana, USA: an example of negative inversion tectonics? In: Cooper, M.A., Williams, G.D. (Eds.), Inversion Tectonics. Geological Society of London Special Publication, pp. 223–234.

Ramsay, J.G., Huber, M.I., 1983. The Techniques of Modern Structural Geology. Vol. 1: Strain Analysis. Academic Press, London.

Ramsay, J.G., Huber, M.I., 1987. The Techniques of Modern Structural Geology. Vol. 2: Folds and Fractures. Academic Press, London.

Rowe, K.J., Rutter, E.H., 1990. Paleostress estimation using calcite twinning: experimental calibration and application to nature. Journal of Structural Geology 12, 1–18.

Sibson, E.H., 1977. Fault rock and fault mechanisms. Journal of Geological Society of London 133, 191–213.

Sibson, R.H., 1990. Conditions for fault-valve behaviour. In: Knipe, R.J., Rutter, E.H. (Eds.), Deformation Mechanisms, Rheology and Tectonics. Geological Society of London Special Publication 54, pp. 15–28.

Travè, A., Labaume, P., Calvet, F., Solder, A., Tritlla, J., Buatier, M., Potdevin, J., Seguret, M., Raynaud, S., Brisqueu, L., 1998. Fluid migration during Eocene thrust emplacement in the south Pyrenean foreland basin (Spain): an integrated structural mineralogical and geochemical approach. In: Mascle, A., Puigdefabregans, C., Lutherbacher, H.P., Fernandez, M. (Eds.), Cenozoic Foreland Basin of Western Europe. Geological Society Special Publication 134, pp. 163–188.

Turner, F.J., Griggs, D.T., Heard, H.C., 1954. Experimental deformation of calcite crystals. Bulletin Geological Society of America 65, 883–934.

Vannucchi, P., 2001. Monitoring paleo-fluid pressure through vein micro-structures. Journal of Geodynamics 32, 567–581.

Vannucchi, P., Maltman, A.J., 2000. Insight into shallow-level process of mountain building from Northern Apennines, Italy. Journal of Geological Society, London 157, 105–120.

Wennberg, O.P., 1996. Superimposed fabrics due to reversal of shear sense: an example from the Bergen Arc Shear Zone, western Norway. Journal of Structural Geology 18 (7), 871–889.

Williams, G.D., Powell, C.M., Cooper, M.A., 1989. Geometry and kinematics of inversion tectonics. In: Cooper, M.A., Williams, G.D. (Eds.), Inversion Tectonics Special Publication, Geological Society of London 44, pp. 3–15.

Worley, B.A., Wilson, C.J.L., 1996. Deformation partitioning and foliation reactivation during transpressional orogenesis, an example from the Central Longmen Shan, China. Journal of Structural Geology 18, 395–411.